Title
Photochemical intermolecular dearomative cycloaddition of bicyclic azaarenes with alkenes

Journal
Science, 371(6536)

ISSN
0036-8075

Authors
Ma, Jiajia
Chen, Shuming
Bellotti, Peter
et al.

Publication Date
2021-03-26

DOI
10.1126/science.abg0720

Peer reviewed

Published in final edited form as:
Science. 2021 March 26; 371(6536): 1338–1345. doi:10.1126/science.abg0720.

Photochemical Intermolecular Dearomative Cycloaddition of Bicyclic Azaarenes with Alkenes

Jiajia Ma[#1], **Shuming Chen**[#2], **Peter Bellotti**[#1], **Renyu Guo**[3], **Felix Schäfer**[1], **Arne Heusler**[1], **Xiaolong Zhang**[1], **Constantin Daniliuc**[1], **M. Kevin Brown**[3,*], **Kendall N. Houk**[2,*], **Frank Glorius**[1,*]

[1]Organisch-Chemisches Institut, Westfälische Wilhelms-Universität Münster, Corrensstrasse 40, 48149 Münster, Germany

[2]Department of Chemistry and Biochemistry, University of California, Los Angeles, California 90095-1569, United States

[3]Department of Chemistry, Indiana University, Bloomington, Indiana 47405, United States

[#] These authors contributed equally to this work.

Abstract

Dearomative cycloaddition reactions represent an ideal means of converting flat arenes into three dimensional architectures of increasing interest in medicinal chemistry. Quinolines, isoquinolines and quinazolines, despite containing latent diene and alkene subunits, are scarcely applied in cycloaddition reactions, due to inherent low reactivity of aromatic systems and selectivity challenges. Here we disclose an energy-transfer mediated, highly regio- and diastereoselective intermolecular [4+2] dearomative cycloaddition reaction of these bicyclic azaarenes with a plethora of electronically-diverse alkenes. This approach bypasses the general reactivity and selectivity issues, thereby providing various bridged polycycles which previously have been inaccessible or required elaborate synthetic efforts. Computational studies with density functional theory elucidate the mechanism and origins of the observed regio- and diastereoselectivities.

Advancing efficient and selective catalytic processes to access modular structural complexity is a central theme of modern organic synthesis (1, 2). Cycloaddition reactions are among the most synthetically useful means to meet this end by leveraging the construction of sophisticated architectures from readily available feedstocks, and feature excellent step/atom economy with predictable and exclusive stereoselectivity (Fig. 1A) (3, 4). Therefore, cycloaddition reactions have played a prominent role in synthetic chemistry and constitute a major theme in chemistry education (5). The classical substrates employed in cycloaddition reactions are unsaturated hydrocarbons such as 1,3-butadienes, alkenes, alkynes and other

[*]Correspondence to: brownmkb@indiana.edu, houk@chem.ucla.edu, glorius@uni-muenster.de.

Author contributions

F.G., M.K.B. and J.M., R.G. conceived the project. J.M. and R.G. discovered the HFIP and $BF_3{\cdot}OEt_2$ conditions, independently. J.M., P.B., R.G., F.S., A.H. and X.Z. performed the synthetic experiments. S.C. performed the DFT calculations. C.D. analyzed the X-ray structures. J.M., S.C., M.K.B., K.N.H. and F.G. supervised the research and wrote the manuscript with contributions from all authors.

Competing interests

The authors declare no competing interests.

Europe PMC Funders Author Manuscripts

related compounds. Industrially, these unsaturated hydrocarbons are produced stepwise *via* petroleum refining to afford saturated hydrocarbons, followed by cracking or dehydrogenation under harsh conditions (6). However, the initial refining can also directly afford unsaturated N-heterocycles, such as quinoline, isoquinoline and quinaldine. Despite containing both latent diene and alkene subunits, these bicyclic azaarenes have shown dramatically limited applications in cycloaddition reactions. This phenomenon can be attributed both to the severe reactivity challenges and selectivity issues towards the intermolecular dearomative cycloaddition (DAC) reaction (7–10). First, overcoming the kinetic barrier of DAC reactions has traditionally required harsh conditions (Fig. 1B, dashed curve) or an extremely reactive or tailored cycloaddend (11–14). Second, the dearomative cycloadditions are endergonic processes due to the breaking of aromaticity, 81.0 kcal·mol^{-1} for quinoline and 76.5 kcal·mol^{-1} for quinazoline (15), thus under thermally induced reaction conditions the starting materials will be favored and a reverse reaction is feasible (Fig. 1B, dashed curve). Last, even if the kinetic and thermodynamic issues could be overcome, the inherent severe chemo-, regio- and diastereoselectivity challenges would still diminish the broad utility of such methods (Fig. 1C).

In this context, an energy transfer (EnT) approach paves the way towards the solution of the aforementioned reactivity and selectivity problems (16–18). Initially, the ground state azaarene could be selectively excited to a higher energy triplet state by EnT process, thus leading to a compressed kinetic barrier compared to the thermally controlled pathway (Fig. 1B, solid curve *vs* dashed curve). Moreover, the combination of significantly higher triplet energies in the terminal dearomatization products (which are thus not amenable to further EnT) and the sufficiently mild conditions prevents the reverse reaction. Compared to the conventional ground state chemistry, the unconventional triplet state intermediate could potentially lead to unexpected chemo-, regio- and diastereoselectivities. Recent works have demonstrated the application of EnT process for enabling dearomative cycloaddition reactions, but have faced large limitations. As such, the reaction has mostly been limited to electron-rich arenes or their prefunctionalized derivatives, and intramolecular variants (Fig. 1D), which require multi-step substrate synthesis and offer limited generality (19–27). Additionally, inferior selectivity has been observed in both the intra- and intermolecular DAC reactions (Fig. 1D). All these limitations are also commonly encountered under the thermally-controlled DAC reactions (28–33). Herein, we apply EnT process in combination with Brønsted or Lewis acid mediators to enable the selective DAC reaction of simple quinolines, isoquinolines and quinazolines with a broad variety of alkenes (Fig. 1E). This reaction features exclusive carbocyclic [4+2] cycloaddition, high/divergent regioselectivity and excellent *endo*-diastereoselectivity.

Evaluation of reaction conditions

Initial experiments involved the reaction of quinoline **1a** and 1-hexene **2a** in the presence of the commercially available photosensitizer [Ir-F] ([Ir(*d*F(CF$_3$)ppy)$_2$(dtbbpy)](PF$_6$), 1 or 2 mol%) under the irradiation of blue LEDs (Fig. 2A-2B and fig. S1-S2). Under condition **A** with HFIP as the solvent, both regiomers **3a** (*syn*: R^2 close to the nitrogen of product) and **3b** (*anti*: the reverse cycloaddition order) were isolated in comparable yields of 41% and 46%, but with excellent *endo*-diastereoselectivities (entry 1, Fig. 2B). By applying condition

B with CH_2Cl_2 as the solvent and $BF_3{\cdot}OEt_2$ (1.25 equiv.) as an additive, **3b** was obtained as the predominant regiomer over **3a** (entry 2). Next, when using 6-methyl quinoline **1b**, under condition **B**, two regiomers **4a** and **4b** were obtained (entry 4). Interestingly, back to condition **A**, a single regiomer **4a** was isolated in excellent yield (88%) and as a single *endo*-diastereomer (entry 5), while the other regiomer **4b** was not detected by crude ^{1}H NMR analysis. By using 4-methyl-1-pentene (**2b**), a single regiomer **5a** was also obtained with good outcome (entry 6). Styrene (**2c**) was also compatible and provided a single regioisomeric product **6a** with comparable results (entry 7). Both the unactivated alkene **2a-b** and the activated one **2c** lead to the consistent *endo*- diastereoselectivity of products **3-6**. Excluding the acidic components, $BF_3{\cdot}OEt_2$ or HFIP, respectively, completely suppressed product formation (entries 3 and 8). Overall, regarding both the reaction efficiency and selectivity, condition **A** with HFIP as Brønsted acid mediator was assessed to be optimal for the substituted quinoline **1b** while condition **B** with $BF_3{\cdot}OEt_2$ as Lewis acid mediator was more suitable for the unsubstituted substrate (**1a**).

Mechanistic investigation

The influence of the acidic solvent HFIP (34–35) and the additive $BF_3{\cdot}OEt_2$ on both the reaction efficiency and selectivities indicates the pivotal role of the Brønsted (36) and Lewis (37–38) acids. Taking this into account, we hypothesized that either the solvent HFIP or the additive $BF_3{\cdot}OEt_2$ was binding to the quinolines **1a** and **1b** through hydrogen-bonding or Lewis acid/base interaction, respectively, to give an intermediate **I**, characterized by markedly decreased triplet energy (Fig. 2A). Intermediate **I** can then be selectively excited to the corresponding triplet state (**II**) by EnT process. The resultant highly reactive biradical intermediate **II** would then add across an alkene in a regio- and stereoselective fashion, thus affording the [4+2] DCA products **3-6**. A number of mechanistic experiments support this scenario (Fig. 3A, see supplementary materials for details). First, control experiments using H-bonding acceptor co-solvents such as 1,4-dioxane, acetonitrile and *N,N*-dimethylacetamide (DMA) with HFIP, led to remarkable decrease of the reaction efficiency (table S8). Second, the H-bonding between HFIP and quinoline **1b** in solution is supported by a series of NMR experiments including ^{1}H NMR titration, NOESY and Job-plot analysis (fig. S3–S9). Third, in the solid state, a dual H-bonding interaction is directly observed in the co-crystal structure of quinoline-2-carboxylate (**1c**) and HFIP (Fig. 3A and fig. S22). These observations strongly support an H-bonding interaction between the nitrogen atom of quinoline and the alcoholic proton of HFIP. The Lewis acid/base interaction between $BF_3{\cdot}OEt_2$ and quinolines has been previously disclosed (39). The proposal of these interactions to decrease the singlet-triplet energy gap was confirmed by density functional theory (DFT) calculations. Accordingly, triplet energy of **1a** is calculated to be 61.7 kcal·mol^{-1}. In contrast, after complexation with HFIP, protonation by HCl or interaction with BF_3, decreased triplet energies of 61.2, 57.7 and 58.9 kcal·mol^{-1} are respectively predicted, rendering these adducts more amenable to energy transfer by the photosensitizer [Ir-F] (60.8 kcal·mol^{-1}) (fig. S14-S15). This effect of Brønsted and Lewis acids on the triplet energy of quinolines is consistent with the experimental results (Fig. 2B, entries 3 and 8). Next, the proposed EnT activation of quinoline **1b** by the excited photosensitizer [Ir-F] was supported by Stern-Volmer luminescence quenching analysis, since a competitive single electron

transfer (SET) event was found to be thermodynamically unfeasible by cyclic voltammetry study (fig. S10-12). Conversely, the suggested energy transfer (EnT) process was further corroborated by the correlation of the reaction rate to triplet energies rather than the redox potentials of various photosensitizers (table S10). Overall, both the experimental and computational studies suggest that the ground state quinolines can be activated through Brønsted/Lewis acids mediated EnT process, which is the key for success of the [4+2] DAC reaction.

The high levels of regio- and stereocontrol observed for unactivated alkenes were of particular interest. We initially hypothesized that spin densities of the substrate in the triplet state would have a significant impact on free energy barriers. While calculated spin densities showed that *N*-protonation and coordination generally lead to increased spin density at the 5-position for quinoline **1b** in the triplet state (fig. S13), rate-determining C–C forming transition states (TSs) for the formal [4+2] reaction between quinoline **1b** and alkene **2b** exhibited low regioselectivity ($\Delta\Delta G^{\ddagger}$ 0.4–0.5 kcal·mol^{-1}) when calculated in the gas-phase (Fig. 3B), indicating that regiocontrol is not solely due to differences in spin densities. The inclusion of an implicit solvent model for HFIP greatly increases the predicted regioselectivity to levels in good agreement with experimental observations ($\Delta\Delta G^{\ddagger}$ 1.5-1.7 kcal·mol^{-1}). These results suggest that TS polarity and solvent stabilization play an important role in enforcing regiocontrol. Calculated TS dipole moments confirm that **TS-1a**, the TS leading to the major product isomer **5a**, is significantly more polar (11.4 Debye in HFIP) compared to regioisomeric TSs **TS-1c** (9.1 Debye) and **TS-1d** (9.4 Debye). In all four TSs, a close, stabilizing interaction (2.55–2.68 Å) is observed between the developing SOMO of quinoline **1b** and one of the allylic C–H bonds on **2b**, which anchors the approaching alkene and shapes the lowest-energy TS geometry. As a result, a destabilizing steric clash (H...H distance 2.28 Å) exists between the approaching alkene and the methyl substituent on quinoline **1b** in **TS-1b**. This steric clash is absent from the **TS-1a**, contributing to the high diastereoselectivity ($\Delta\Delta G^{\ddagger}$ 2.0 kcal·mol^{-1}). The effects of dispersion were calculated to be insignificant for this reaction (see supplementary material). Calculated selectivities for the reaction between **1b** and styrene (**2c**) found similarly good agreement with experimental observations, with **π-π** stacking as an important determining factor of TS geometries and energies (fig. S20).

Scope of the [4+2] DAC reaction

Having assessed the feasibility of the dearomative approach, the reaction scope with respect to the bicyclic azaarenes was evaluated (Fig. 4). In general, the quinolines bearing substituents at each of the 2-8 positions are compatible in this [4+2] dearomative cycloaddition reaction. Accordingly, under condition **B**, 2, 3 or 4-alkyl substituted quinolines were converted to the corresponding dearomatization products **7-10** in good yields, regio- and diastereoselectivities. Condition **A** was applied for the 5, 6, 7 or 8-substituted quinolines, thus giving the products **11-31** with remarkable regio- and diastereocontrol. The *anti*-regioselectivity was observed as predominant when using 2, 3, 4, 5 or 7-substituted quinolines (products **7-11**, **13** and **15**). A reverse order of addition (*syn*-regioselectivitv) occurred when using 6 or 8-substituted quinolines (products **12**, **14** and

16-31). HCl (2 equiv.) was added to accelerate the reaction or to promote the conversion of the less reactive 5 or 8 positions substituted quinolines (products **11**, **14** and **15**, table S5-S7). 6-Hydroxyquinoline proved amenable to the [4+2] DAC reaction by providing a ketone **29** through the tautomerization of an enol intermediate. Likewise, both isoquinolines and quinazolines showed good compatibility in the [4+2] DAC reaction (products **32-44**). As a limitation, when 1-methyl isoquinoline was applied in this transformation, two separable regiomers **37a** and **37b** were afforded with modest levels of diastereoselectivity. With respect to quinazolines, the *syn*-regioselectivity was commonly observed (products **38-42**). However, when 4-aryl quinazolines were used as substrates, the reverse *anti*-regiomers became predominant (**43b**/**44b** *vs* **43a**/**44a**).

A quite broad scope of unactivated and activated alkenes proved amenable substrates, as presented in Fig. 5. Excellent functional group compatibility was observed, such as bromo (**49**), esters (**50**), nitrile (**51**), aldehyde (**52**), hydroxyl (**53**), carboxylic acid (**54**), phosphate (**55**), silane (**56**), sulfonamide (**57**), phthalimide (**58**), poly-fluorinated alkane or arene (**59**, **60**), benzothiophene (**61**), pyrazine (**64**), and many bioactive motifs (**62-63** and **65-66**). The [4+2] DAC reaction also proceeded efficiently with gaseous propene (2 bar), thus giving **48** in 58% yield as a single regiomer and diastereomer. A gram scale reaction was performed using 6-methyl quinoline and 1-octene to afford 1.46 g of **45** (5.73 mmol, 82% yield, >95:5 r.r. and >95:5 d.r.), (see detailed step-by-step protocol in the supplementary materials). An internal alkene, *trans*-1,2-dichloroethylene was also compatible and gave the target product as two separable diastereomers **67a** and **67b**. Aiming at the construction of challenging all-carbon quaternary stereocenters, 5-methyl quinoline was coupled with a plethora of alkenes under condition **B** thus providing the corresponding products (**68-70**) with good yields and selectivities. Stereoconvergence was observed when using *trans*- or *cis*-3-hexene, respectively, thus consistently leading to the product **71** with excellent *trans*-diastereoselectivity. *cis*-Cyclooctene was applicable to provide **72** in 92% yield and with good *trans*-diastereoselectivity (90:10). In contrast, unsymmetrical 1,2-disubstituted alkenes displayed decreased selectivity towards the corresponding products. Trisubstituted and tetrasubstituted alkenes proved not compatible with this transformation (table S11-S12). Various electronically diverse styrenes, *O*-vinyl esters and *N*-vinvl amides are also applicable in the [4+2] DAC reaction (products **73-89**), providing excellent levels of both regio- and diastereocontrol. X-ray structures of **75** and **81** are presented to confirm the configuration of the products. A complementary scope of alkenes is available in the supplementary materials (table S13). Additionally, to improve the user-friendliness and enhance the reproducibility of this method, an assessment of the condition-based sensitivity was performed (40). As a result, this reaction was found to be comparatively sensitive to oxygen and high temperature. A slightly decreased yield was observed when the reaction was scaled up by 70 times, albeit under reduced photosensitizer loading. In contrast, the concentration of substrates, moisture and light intensity did not show any remarkable influence on the reaction (fig. S21).

Synthetic applications

Next, derivatization of the obtained [4+2] DAC products towards relevant three-dimensional scaffolds was conducted (Fig. 6A). Starting from **23**, chemoselective reduction were performed under D2 atmosphere (1 atm) or H_2 (50 bar), thus affording a deuterated tetrahydro 5,8-ethanoquinoline **90** or a fully saturated decahydro 5,8-ethanoquinoline **91**, respectively. Compound **23** could also be converted to the pyridine *N*-oxide **92** by chemoselective *meta*-chloroperbenzoic acid (*m*CPBA) oxidation, without epoxidation of the remaining C=C double bond. All these motifs are accompanied by a pharmaceutically appealing fluorinated quaternary stereocenter which has been readily introduced by the [4+2] DAC reaction using commercial 8-fluoroquinoline. The poly-chlorinated dearomatization product **30** can undergo a dechlorination-reduction reaction to give **93**. The alkenyl chloride of **30** was chemoselectively coupled with 4-fluorophenylboronic acid — overcoming the presence of the heteroaryl chloride — under palladium catalysis. Followed by facile hydrogenation, **94** was afforded in 80% yield over two steps and as a single diastereomer. Starting from the amide-containing dearomatization products **86** and **87**, a sequential two-step reduction reaction provided a secondary amine **95** and a tertiary one **96**, respectively. Likewise, an alcohol **97** was produced by a convenient hydrolysis of compound **80**. To emphasize the applicability of this [4+2] DAC reaction towards biologically active compounds, the shortened synthesis of a thromboxane A_2/prostaglandin H_2 receptor antagonist (**121**) is presented (Fig. 6B) (41). Accordingly, the dearomatization product **37a** was reduced and hydrolyzed in a one-pot reaction to give **98**. A subsequent Barton-McCombie deoxygenation gave **99** as a single diastereomer. Following benzylic bromination, a palladium-catalyzed cross-coupling delivered the target compound **101**. Compared to the original 9-step synthesis from a conventional Diels-Alder reaction product **102**, only 5 steps are needed by starting from the dearomatization product **37a** to access the terminal product **101**. Overall, the [4+2] DAC reaction could provide a direct and efficient access to various functionalized bridged polycycles which previously have been inaccessible or required strenuous synthetic efforts.

Given the emerging interest in bridged polycycles emerging in medicinal chemistry (42, 43), we anticipate this method will find substantial use in facilitating the efficient synthesis of such scaffolds.

Supplementary Material

Refer to Web version on PubMed Central for supplementary material.

Acknowledgments

J.M. thanks Dr. X. Huang (UIUC), Dr. J. Li, S. Mondal, T. Pinkert, T. Paulisch and F. Strieth-Kalthoff (all WWU) for assistance and discussions.

Funding

Generous financial support by the European Research Council (ERC Advanced Grant Agreement no. 788558) and the Deutsche Forschungsgemeinschaft (SFB 858, Leibniz Award) is gratefully acknowledged. M.K.B. and R.G. thank National Institutes of Health (R35GM131755) for financial support. K.N.H thanks the National Science Foundation (Grant CHE-1764328) for financial support. Calculations were performed on the Hoffman2 cluster at

the University of California, Los Angeles, and the Extreme Science and Engineering Discovery Environment (XSEDE), which is supported by the National Science Foundation (Grant OCI-1053575).

Data and materials availability

Characterization of new compounds and detailed reaction optimization and mechanistic studies are provided in the supplementary material; crystallographic data are available free of charge under CCDC reference numbers 2041010 (intermediate **I'**), 2060268 (**71**·MeI), 2041012 (**75**), 2041013 (**81**) and 2041014 (**89**·HCl).

References and Notes

1. Trost B. The atom economy-a search for synthetic efficiency. Science. 1991; 254:1471–1477. [PubMed: 1962206]
2. Wender PA, Verma VA, Paxton TJ, Pillow TH. Function-oriented synthesis, step economy, and drug design. Acc Chem Res. 2008; 41:40–49. [PubMed: 18159936]
3. Jørgensen, KA. Cycloaddition reactions in organic synthesis. John Wiley & Sons; 2002.
4. Carruthers, W. Cycloaddition reactions in organic synthesis. Elsevier; 2013.
5. Nicolaou KC, Snyder SA, Montagnon T, Vassilikogiannakis G. The Diels-Alder reaction in total synthesis. Angew Chem Int Ed. 2002; 41:1668–1698.
6. Weissermel, K, Arpe, H-J. Industrial organic chemistry. John Wiley & Sons; 2008.
7. Atherton J, Jones S. Diels-Alder reactions of anthracene, 9-substituted anthracenes and 9,10-disubstituted anthracenes. Tetrahedron. 2003; 46:9039–9057.
8. Remy R, Bochet CG. Arene-alkene cycloaddition. Chem Rev. 2016; 116:9816–9849. [PubMed: 27340900]
9. Zheng C, You S-L. Catalytic asymmetric dearomatization by transition-metal catalysis: a method for transformations of aromatic compounds. Chem. 2016; 1:830–857.
10. Wertjes WC, Southgate EH, Sarlah D. Recent advances in chemical dearomatization of nonactivated arenes. Chem Soc Rev. 2018; 47:7996–8017. [PubMed: 30073226]
11. Siddiqi Z, Wertjes WC, Sarlah D. Chemical equivalent of arene monooxygenases: dearomative synthesis of arene oxides and oxepines. J Am Chem Soc. 2020; 142:10125–10131. [PubMed: 32383862]
12. Leitch JA, Rogova T, Duarte F, Dixon DJ. Dearomative photocatalytic construction of bridged 1,3-diazepanes. Angew Chem Int Ed. 2020; 59:4121–4130.
13. Preindl J, Chakrabarty S, Waser J. Dearomatization of electron poor six-membered N-heterocycles through [3 + 2] annulation with aminocyclopropanes. Chem Sci. 2017; 8:7112–7118. [PubMed: 29147541]
14. Xiong Q, Dong S, Chen Y, Liu X, Feng X. Asymmetric synthesis of tetrazole and dihydroisoquinoline derivatives by isocyanide-based multicomponent reactions. Nat Commun. 2019; 10:2116. [PubMed: 31073191]
15. Bird CW. The relationship of classical and magnetic criteria of aromaticity. Tetrahedron. 1996; 52:9945–9952.
16. Strieth-Kalthoff F, James MJ, Teders M, Pitzer L, Glorius F. Energy transfer catalysis mediated by visible light: principles, applications, directions. Chem Soc Rev. 2018; 47:7190–7202. [PubMed: 30088504]
17. Zhou Q-Q, Zou Y-Q, Lu L-Q, Xiao W-J. Visible-light-induced organic photochemical reactions through energy-transfer pathways. Angew Chem Int Ed. 2019; 58:1586–1604.
18. Strieth-Kalthoff F, Glorius F. Triplet energy transfer photocatalysis: unlocking the next level. Chem. 2020; 6:1888–1903.
19. Strieth-Kalthoff F, Henkel C, Teders M, Kahnt A, Knolle W, Gómez-Suárez A, Dirian K, Alex W, Bergander K, Daniliuc CG, Abel B, et al. Discovery of unforeseen energy-transfer-based transformations using a combined screening approach. Chem. 2019; 5:2183–2194.

20. James MJ, Schwarz JL, Strieth-Kalthoff F, Wibbeling B, Glorius F. Dearomative cascade photocatalysis: divergent synthesis through catalyst selective energy transfer. J Am Chem Soc. 2018; 140:8624–8628. [PubMed: 29961335]
21. Zhu M, Zheng C, Zhang X, You S-L. Synthesis of cyclobutane-fused angular tetracyclic spiroindolines via visible-light-promoted intramolecular dearomatization of indole derivatives. J Am Chem Soc. 2019; 141:2636–2644. [PubMed: 30653315]
22. Ma J, Strieth-Kalthoff F, Dalton T, Freitag M, Schwarz JL, Bergander K, Daniliuc C, Glorius F. Direct dearomatization of pyridines via an energy-transfer-catalyzed intramolecular [4+2] cycloaddition. Chem. 2019; 5:2854–2864.
23. Zhu M, Huang X-L, Xu H, Zhang X, Zheng C, You S-L. Visible-light-mediated synthesis of cyclobutene-fused indolizidines and related structural analogs. CCS Chem. 2020:652–664.
24. Oderinde MS, Mao E, Ramirez A, Pawluczyk J, Jorge C, Cornelius LAM, Kempson J, Vetrichelvan M, Pitchai M, Gupta A, Gupta AK, et al. Synthesis of cyclobutane-fused tetracyclic scaffolds via visible-light photocatalysis for building molecular complexity. J Am Chem Soc. 2020; 142:3094–3103. [PubMed: 31927959]
25. Zhang Z, Yi D, Zhang M, Wei J, Lu J, Yang L, Wang J, Hao N, Pan X, Zhang S, Wei S, et al. Photocatalytic intramolecular [2 + 2] cycloaddition of indole derivatives via energy transfer: a method for late-stage skeletal transformation. ACS Catal. 2020; 10:10149–10156.
26. Rolka AB, Koenig B. Dearomative cycloadditions utilizing an organic photosensitizer: an alternative to iridium catalysis. Org Lett. 2020; 22:5035–5040. [PubMed: 32567316]
27. Zhu M, Zhang X, Zheng C, You S-L. Visible-light-induced dearomatization via [2+ 2] cycloaddition or 1, 5-hydrogen atom transfer: divergent reaction pathways of transient diradicals. ACS Catal. 2020; 10:12618–12626.
28. Miura T, Funakoshi Y, Murakami M. Intramolecular dearomatizing [3 + 2] annulation of α-imino carbenoids with aryl rings furnishing 3,4-fused indole skeletons. J Am Chem Soc. 2014; 136:2272–2275. [PubMed: 24437578]
29. Trost BM, Ehmke V, O'Keefe BM, Bringley DA. Palladium-catalyzed dearomative trimethylenemethane cycloaddition reactions. J Am Chem Soc. 2014; 136:8213–8216. [PubMed: 24874093]
30. Pham HV, Karns AS, Vanderwal CD, Houk KN. Computational and experimental investigations of the formal dyotropic rearrangements of Himbert arene/allene cycloadducts. J Am Chem Soc. 2015; 137:6956–6964. [PubMed: 25961134]
31. Shen L, Zhao K, Doitomi K, Ganguly R, Li Y-X, Shen Z-L, Hirao H, Loh T-P. Lewis acid-catalyzed selective [2 + 2]-cycloaddition and dearomatizing cascade reaction of aryl alkynes with acrylates. J Am Chem Soc. 2017; 139:13570–13578. [PubMed: 28880536]
32. Inami T, Takahashi T, Kurahashi T, Matsubara S. Nickel-catalyzed [5+2] cycloaddition of 10π-electron aromatic benzothiophenes with alkynes to form thermally metastable 12π-electron nonaromatic benzothiepines. J Am Chem Soc. 2019; 141:12541–12544. [PubMed: 31361485]
33. Lee J, Ko D, Park H, Yoo EJ. Direct cyclopropanation of activated N-heteroarenes via site- and stereoselective dearomative reactions. Chem Sci. 2020; 11:1672–1676. [PubMed: 32206287]
34. Colomer I, Chamberlain AER, Haughey MB, Donohoe TJ. Hexafluoroisopropanol as a highly versatile solvent. Nat Rev Chem. 2017; 1:0088.
35. Pozhydaiev V, Power M, Gandon V, Moran J, Lebœuf D. Exploiting hexafluoroisopropanol (HFIP) in Lewis and Brønsted acid-catalyzed reactions. Chem Commun. 2020; 56:11548–11564.
36. Sherbrook EM, Jung H, Cho D, Baik M-H, Yoon TP. Brønsted acid catalysis of photosensitized cycloadditions. Chem Sci. 2020; 11:856–861.
37. Blum TR, Miller ZD, Bates DM, Guzei IA, Yoon TP. Enantioselective photochemistry through Lewis acid–catalyzed triplet energy transfer. Science. 2016; 354:1391–1395. [PubMed: 27980203]
38. Huang X, Meggers E. Asymmetric photocatalysis with bis-cyclometalated rhodium complexes. Acc Chem Res. 2019; 52:833–847. [PubMed: 30840435]
39. Chénard E, Sutrisno A, Zhu L, Assary RS, Kowalski JA, Barton JL, Bertke JA, Gray DL, Brushett FR, Curtiss LA, Moore JS. Synthesis of Pyridine– and Pyrazine–BF3 Complexes and Their Characterization in Solution and Solid State. J Phy Chem C. 2016; 120:8461–8471.

40. Pitzer L, Schäfers F, Glorius F. Rapid Assessment of the Reaction-Condition-Based Sensitivity of Chemical Transformations. Angew Chem Int Ed. 2019; 58:8572–8576.
41. Saha SL, Roche VF, Pendola K, Kearley M, Lei L, Romstedt KJ, Herdman M, Shams G, Kaisare V, Feller DR. Synthesis and in vitro platelet aggregation and TP receptor binding studies on bicyclic 5,8-ethanooctahydroisoquinolines and 5,8-ethanotetrahydroisoquinolines. Biorg Med Chem. 2002; 10:2779–2793.
42. Lovering F, Bikker J, Humblet C. Escape from Flatland: Increasing Saturation as an Approach to Improving Clinical Success. J Med Chem. 2009; 52:6752–6756. [PubMed: 19827778]
43. Mykhailiuk PK. Saturated bioisosteres of benzene: where to go next? Org Biomol Chem. 2019; 17:2839–2849. [PubMed: 30672560]

Europe PMC Funders Author Manuscripts

Europe PMC Funders Author Manuscripts

One Sentence Summary

Photochemical cycloaddition reactions of quinolines, isoquinolines and quinazolines with alkenes are an efficient and selective route to polycyclic heterocycles.

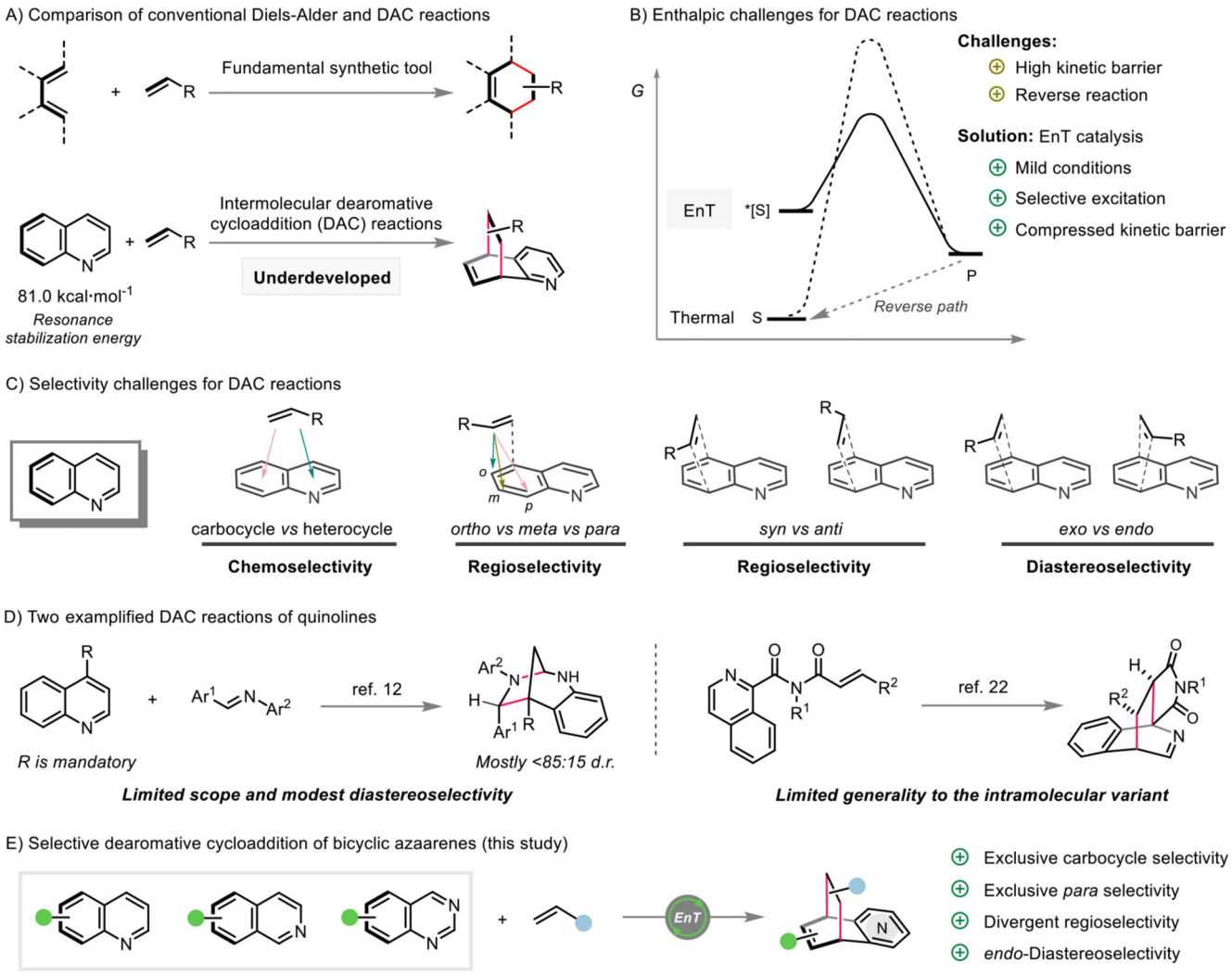

Fig. 1. Dearomative cycloaddition reactions.

A) Comparison of conventional Diels-Alder and DAC reactions. B) Enthalpic challenge for DAC reactions. C) Selectivity challenges for DAC reactions of bicyclic azaarenes. D) Two exemplified DAC reactions of quinolines. E) Selective [4+2] DAC of quinolines, isoquinolines and quinazolines (this study). EnT = energy transfer. S = substrate. P = product.

Europe PMC Funders Author Manuscripts

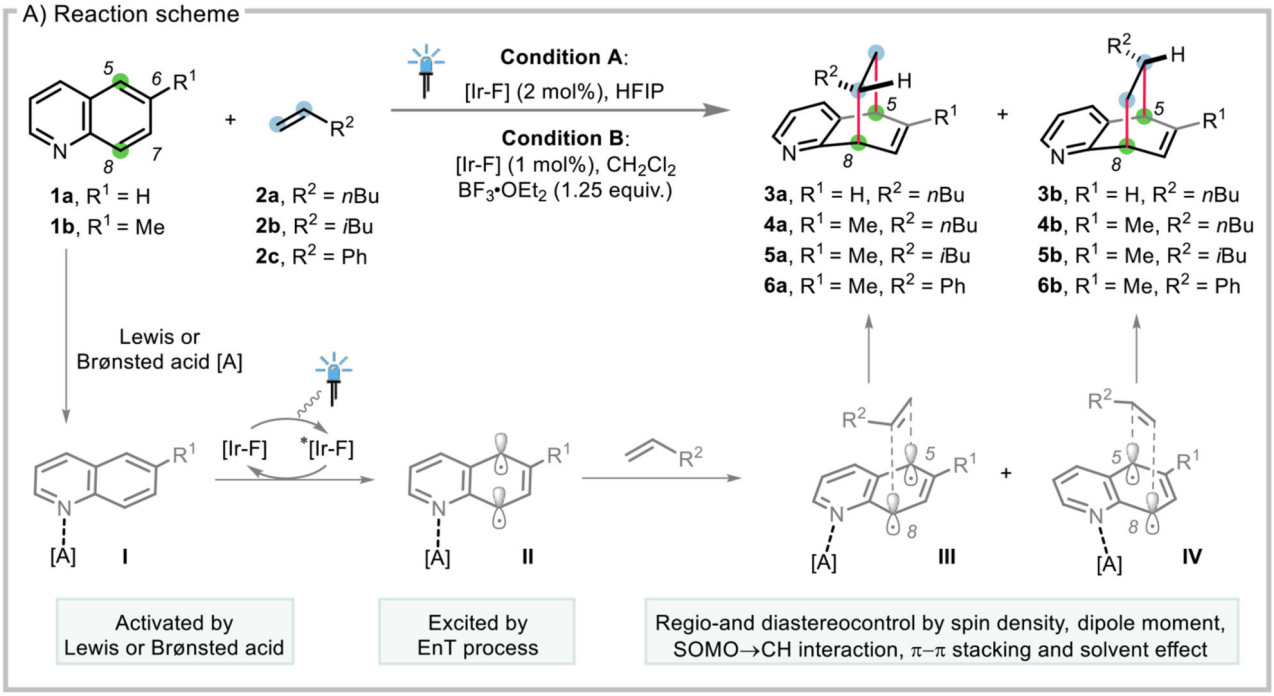

B) Evaluation of conditions

Entry	1a/b	2a-c	Condition	Results
1	**1a**	**2a**	**A**	**3a** (41% yield, >95:5 d.r.); **3b** (46% yield, 94:6 d.r.)
2	**1a**	**2a**	**B**	**3a** (18% yield, 92:8 d.r.); **3b** (78% yield, 83:17 d.r.)
3	**1a**	**2a**	**B** (no BF_3•OEt_2)	**No conversion**
4	**1b**	**2a**	**B**	**4a** (75% yield, 95:5 d.r.); **4b** (18% yield, 83:17 d.r.)
5	**1b**	**2a**	**A**	**4a** (88% yield, >95:5 d.r.); **4b** (not detected)
6	**1b**	**2b**	**A**	**5a** (79% yield, >95:5 d.r.); **5b** (not detected)
7	**1b**	**2c**	**A**	**6a** (71% yield, 95:5 d.r.); **6b** (not detected)
8	**1b**	**2a-c**	**A** (MeOH as solvent)	**No conversion**

Fig. 2. Reaction development.

A) Reaction scheme. B) Conditions evaluation (see table S1-S7). One representative enantiomer of the racemic product is presented for all thorough the text. HFIP = 1,1,1,3,3,3-hexafluoro-propan-2-ol.

Europe PMC Funders Author Manuscripts

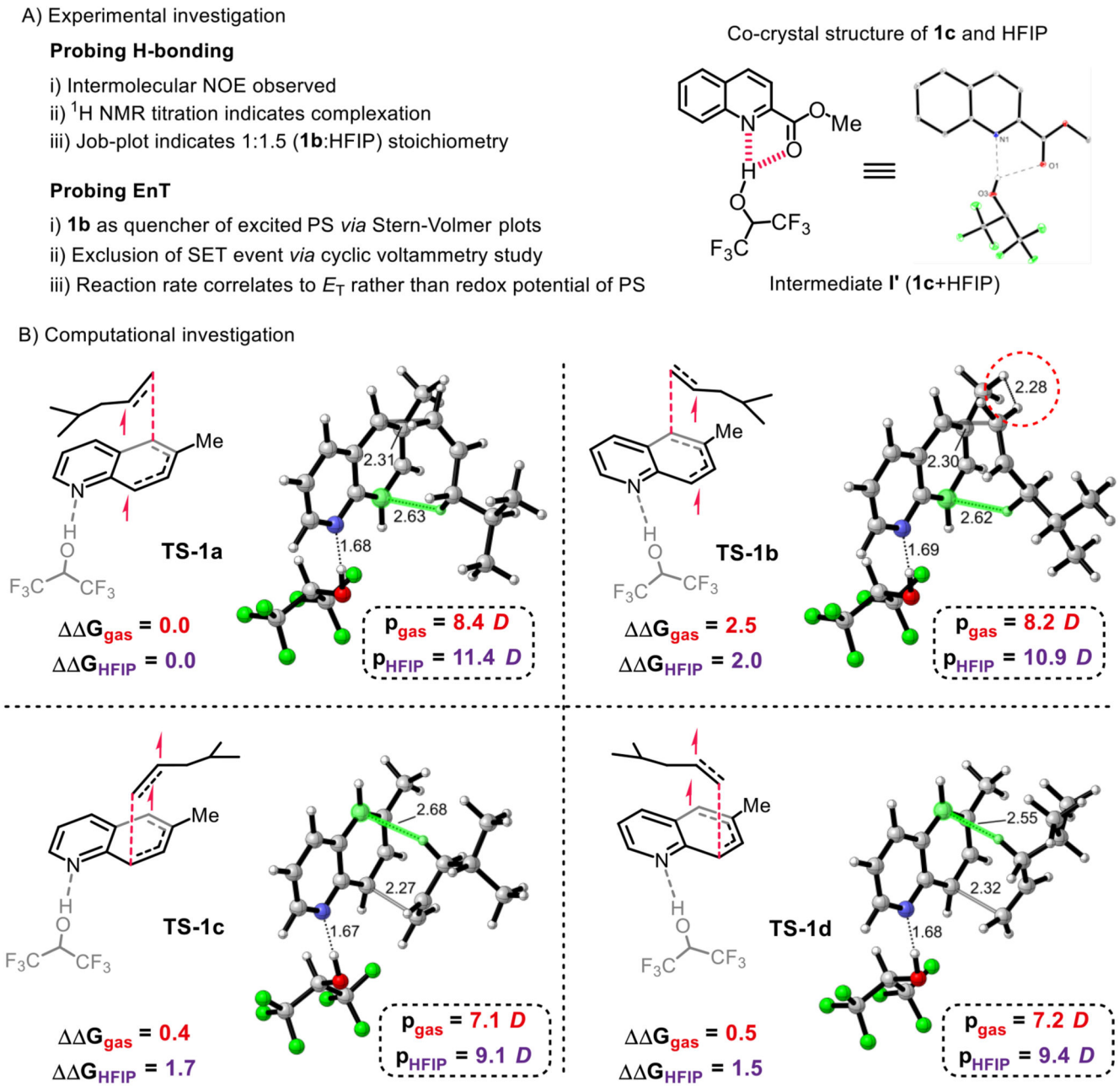

Fig. 3. Mechanistic investigation.

A) Experimental investigation (see fig. S3-S12 and table S8-S10). B) Computational investigation. Calculated C–C forming TS geometries, energies and dipole moments for the [4+2] DCA reaction between triplet 1b and 2b at the ωB97X-D/6-311++G(d,p), SMD (HFIP)//ωB97X-D/6-31G(d), SMD (HFIP) level of theory. Energies are in kcal·mol^{-1}. Interatomic distances are in Å. Green highlights indicate interactions between developing radical SOMOs and allylic C–H bonds. NOE = nuclear overhauser effect. PS = photosensitizer. SET = single electron transfer. D = Debye.

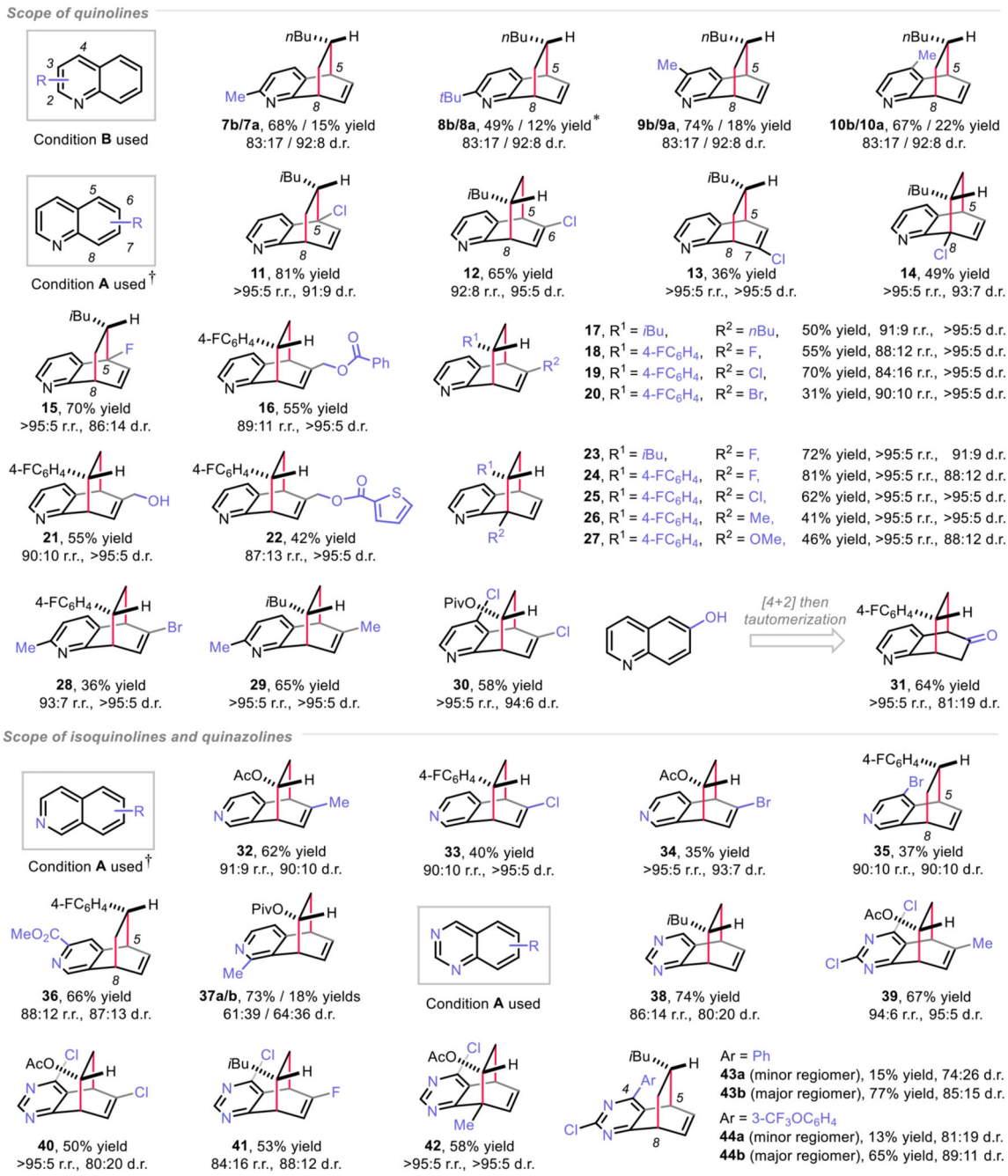

Fig. 4. Scope of bicyclic azaarenes.

*NMR yield of minor regiomer **8a** is presented. †HCl (2 equiv.) was used. Regioisomeric ratio (r.r.) and diastereomeric ratio (d.r.) are determined by crude ^{1}H NMR analysis. For experimental details, see supplementary materials.

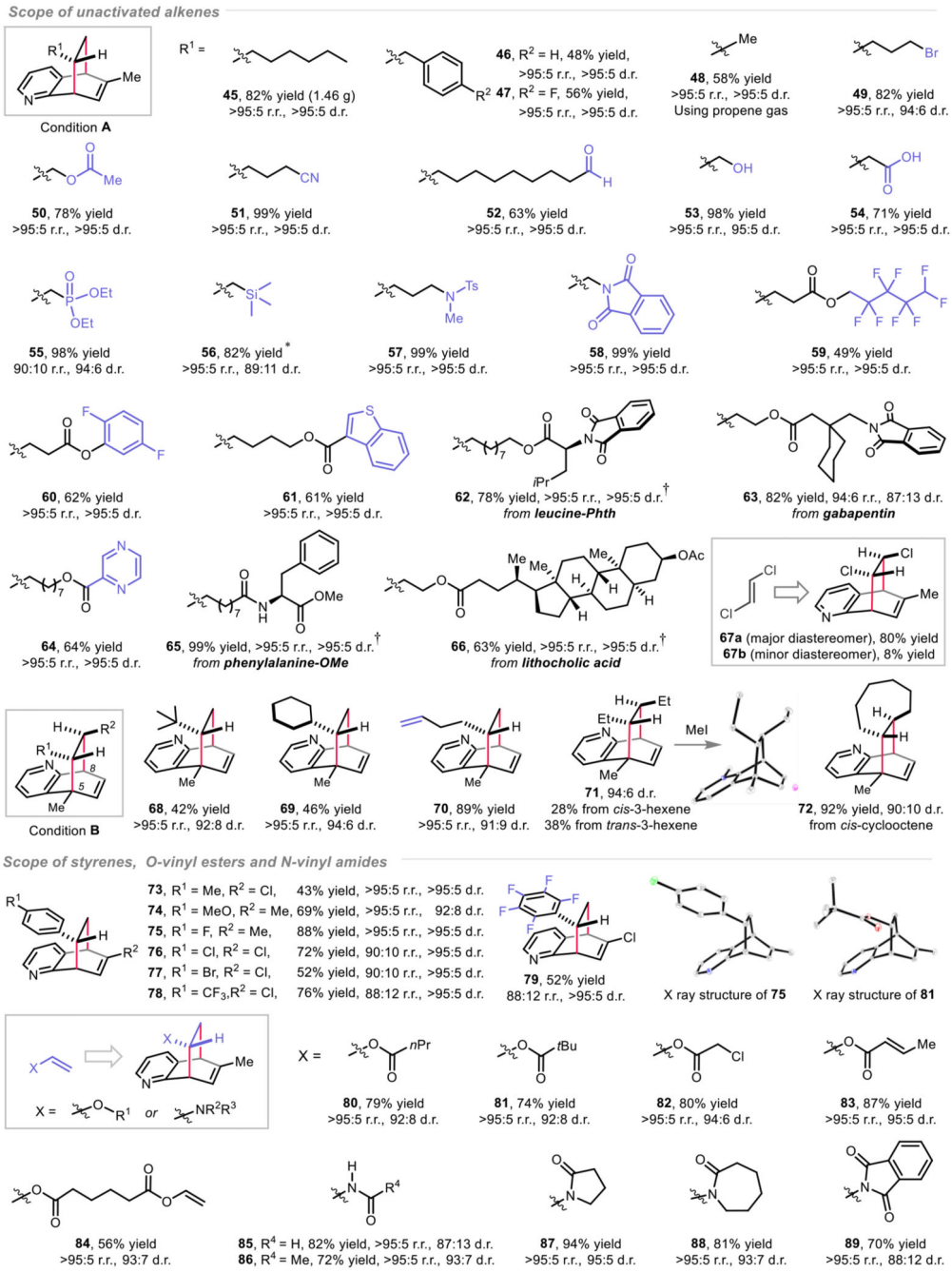

Fig. 5. Scope of alkenes.

*Photosensitizer Ir(*d*F-Me-ppy)$_2$(dtbpy)(PF$_6$) was used. †The d.r. value refers to the [4+2] cycloaddition resulted motif of the product. HCl (2 equiv.) was used for obtaining **46-47**, **57-60**, **62**, **64-65**, **75-84** and **88-89**. Regioisomeric ratio (r.r.) and diastereomeric ratio (d.r.) are determined by crude ^{1}H NMR analysis. For experimental details, see supplementary materials.

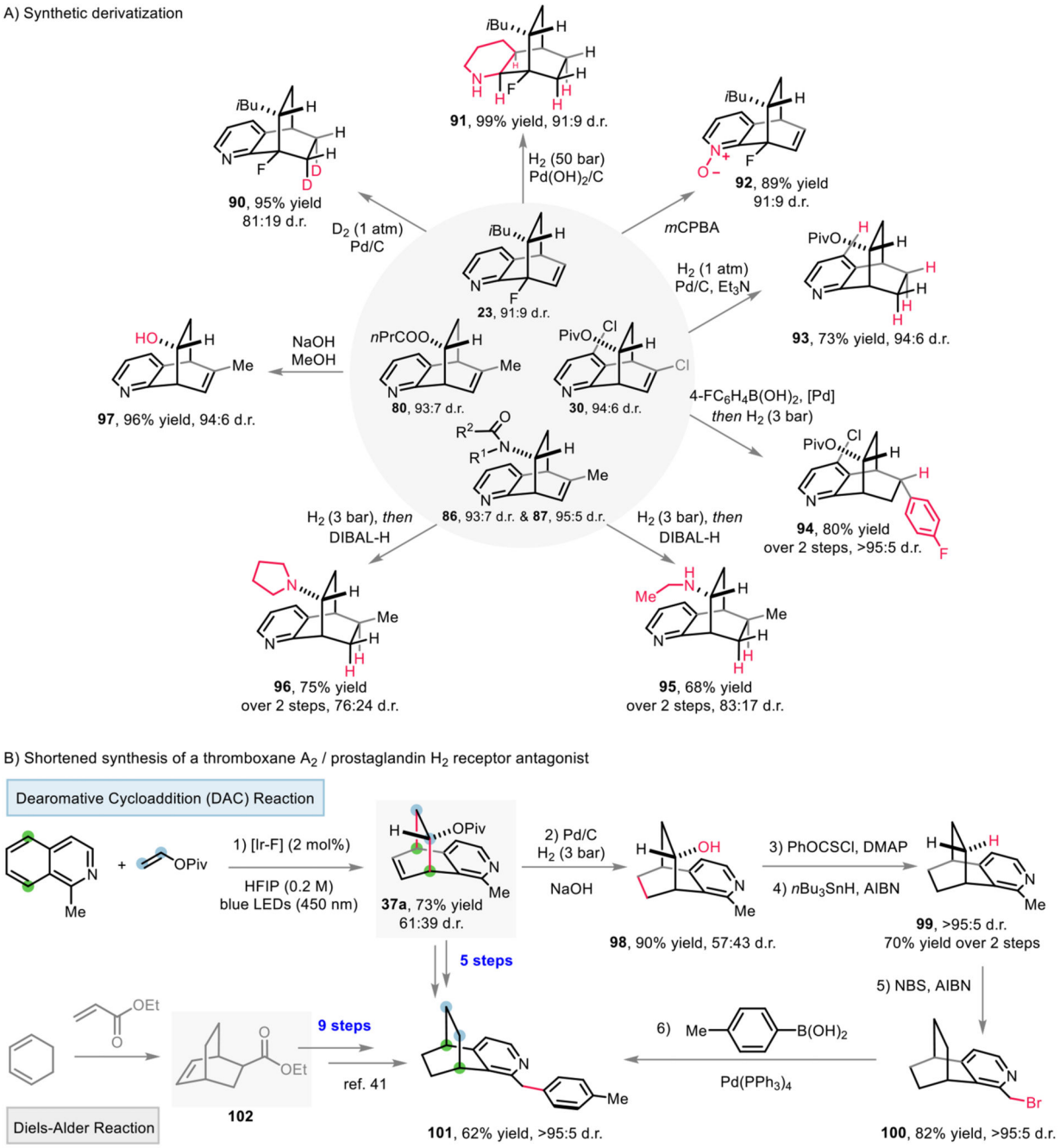

Fig. 6. Synthetic applications.

A) Synthetic derivatization of the [4+2] dearomative cycloaddition products. B) Shortened synthesis of a thromboxane A_2/prostaglandin H_2 receptor antagonist **101**. Diastereomeric ratio (d.r.) displayed herein were determined by ^{1}H NMR analysis of purified compounds. DIBAL-H = diisobutylaluminum hydride. NBS = *N*-bromosuccinimide. AIBN = azobisisobutyronitrile.

Europe PMC Funders Author Manuscripts